ChemComm

COMMUNICATION

View Article Online
View Journal | View Issue

Cite this: *Chem. Commun.*, 2022, **58**, 7558

Received 23rd April 2022,
Accepted 7th June 2022

DOI: 10.1039/d2cc02290g

rsc.li/chemcomm

An iodine-containing probe as a tool for molecular detection in secondary ion mass spectrometry†

Selda Kabatas Glowacki, ‡[ab] Paola Agüi-Gonzalez, ‡[ab] Shama Sograte-Idrissi, [ab] Sebastian Jähne, [b] Felipe Opazo, [a] Nhu T. N. Phan §[ab] and Silvio O. Rizzoli *[ab]

We developed here an iodine-containing probe that can be used to identify the molecules of interest in secondary ion mass spectrometry (SIMS) by simple immunolabelling procedures. The immunolabelled iodine probe was readily combined with previously-developed SIMS probes carrying fluorine, to generate dual-channel SIMS data. This probe should provide a useful complement to the currently available SIMS probes, thus expanding the scope of this technology.

Mass spectrometry imaging (MSI) was introduced to biology a few decades ago, as an imaging technique able to reveal the chemical composition of tissues and cells, and has improved steadily, reaching very high levels of precision.[1–3] To analyse the chemical species on a sample and estimate their abundance, the primary ion beam of a secondary ion mass spectrometer is focused on the surface of the sample, causing the ejection of secondary particles by the impact of the primary ions.[4] A broad spectrum of such instruments is available, with the highest lateral resolutions being provided by the NanoSIMS implementation, at 50 nm or lower.[5] However, the intrinsic nature of such an instrument implies that only mono- or diatomic molecules are detected. Further chemical information is lost, due to the extensive fragmentation induced by the highly reactive primary ion sources (Cs^+/O^-).[6] This problem also affects other SIMS implementations, such as time-of-flight-SIMS (TOF-SIMS), which can reveal molecules only up to ~2.5 kDa.[3]

Thus, labelling particular molecules using SIMS-compatible probes is crucial to detect and visualize larger species, such as proteins. To make this possible, the probes must contain stable elements that are easily ionized, and thus provide a good secondary ion yield. A few different probes fulfilling these requirements have been successfully developed in the last few years. The first investigations employed antibodies linked to heavy metal particles such as gold[7] or lanthanides.[8] Further efforts were then focused on reducing the size of the probes, to go along with the continuous improvements in the spatial resolution of SIMS. Click-chemistry tags containing fluorine or ^{15}N,[9,10] as well as gold nanoparticles- or fluorine-conjugated nanobodies[11,12] have also been successfully applied. Boron-containing probes, developed for the positive secondary ion mode of SIMS, have been recently produced and applied.[13]

However, few multi-targeted proteins SIMS imaging experiments have been performed in the last decades. Due to their low ionization energy,[14] lanthanides are suitable for their detection in the positive ion mode, and enable multi-protein analysis,[8] albeit the large size of their particles limits labelling efficiency. Fluorine or gold are better candidates for the negative ion mode and could be used, in principle, to simultaneously reveal the localization of two proteins of interest with SIMS, but such experiments have not yet been performed. Iodine is the element with the fourth highest electron affinity, after fluorine, chlorine and bromine.[15] Thus, this element represents an excellent choice as SIMS reporter for the negative ion mode and would enable a straightforward strategy for dual-targeted proteins SIMS imaging in the negative secondary ion mode, when combined with another compatible probe. We therefore decided here to develop iodine-conjugated probes for SIMS imaging.

Initially we focused on a precursor molecule with a structure similar to the pentafluorobenzoyl groups in FluorLink, which we developed for NanoSIMS use in the past.[11] However, approaches with pentaiodo-benzoic acid or with reduced iodine content using tetraiodophthalic anhydride and triiodobenzoic acid did not lead to the desired products when coupled to a short peptide at its N-terminus. We had determined iodine loss by ESI-HRMS, which can be explained simply by the lower bond dissociation energy of iodine–carbon bonds and their

[a] *Center for Biostructural Imaging of Neurodegeneration, University Medical Center Göttingen, Von-Siebold-Straße 3a, 37075 Göttingen, Germany. E-mail: srizzol@gwdg.de*
[b] *Department of Neuro and Sensory Physiology, University Medical Center, Göttingen, Humboldtalee 23, 37073 Göttingen, Germany*

† Electronic supplementary information (ESI) available. See DOI: https://doi.org/10.1039/d2cc02290g

‡ Both authors contributed equally to this manuscript.

§ Current address: Department of Chemistry and Molecular Biology, University of Gothenburg, Kemivägen 10, SE-412 96 Gothenburg, Sweden.

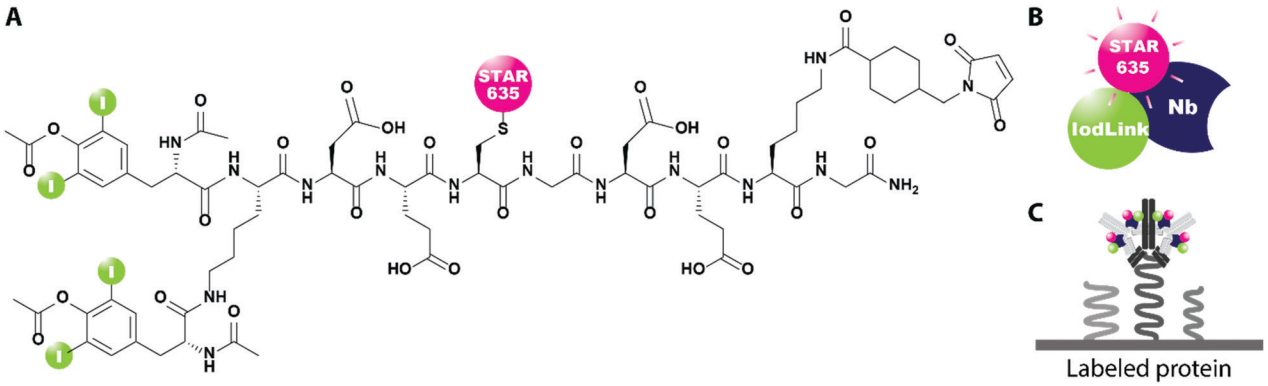

Fig. 1 Schematic representation of immunolabeling of proteins of interest by using IodLink-nanobody anti-mouse κlg. (A) IodLink consists of a soluble peptide with diiodo-L-thyroxine groups on the N-terminus, a fluorophore on the cysteinyl side chain and a maleimide group on the lysine side chain. (B) The thiol-reactive IodLink is conjugated to a secondary nanobody that detects a primary antibody binding the protein of interest. (C) A sequence of primary, secondary and even tertiary antibodies can be used to enhance the signal, increasing the number of IodLink nanobodies in the respective area.

instability under non-inert, oxidative conditions. We therefore searched for iodinated compounds in natural systems and chose diiodo-L-tyrosine, the precursor compound for the synthesis of L-thyroxine, a thyroid hormone essential for vertebrates.[16]

The synthesis was similar to previously published methods,[9–11] beginning with amino acid coupling on a solid support (ESI,† Section S3). The peptide was synthesized from the C- to the N-terminus on an acid-sensitive Sieber amide resin using standard fluorenylmethyloxycarbonyl solid-phase peptide synthesis (Fmoc-SPPS). After coupling of the last amino acid, Fmoc-Lys(Fmoc)-OH, the Fmoc groups were deprotected by basic treatment. Then the commercially available *N*,*O*-diacetyl-3,5-diiodo-L-tyrosine was linked to the two amino groups of the N-terminal lysine. The final peptide was cleaved from the solid support under acidic conditions. In the next step, the fluorophore Star635 maleimide was coupled to the cysteine side chain by a sulfhydryl-maleimide reaction. Finally, a maleimide linker was added to the lysine side chain to generate IodLink with $4x^{127}I$ atoms per molecule (Fig. 1A). Each reaction after solid support was analyzed by HPLC and verified by HR-ESI-MS with no iodine loss observed (ESI,† Section S7). The stability of the iodinated peptide was also confirmed in MALDI-ToF measurements applying different laser powers (ESI,† Section S7). After identification, the products of each step were purified by HPLC to achieve purities of $\geq$95%. IodLink was then conjugated to a secondary nanobody directed against the kappa (κ) light chain of mouse immunoglobulins (κIg), enabling it to be used in immunocytochemistry experiments (ESI,† Section S4) (Fig. 1B). The selected nanobody has two ectopic cysteines that react with IodLink molecules in a sulfydryl-maleimide reaction, resulting in a doubling of the amount of ^{127}I per detected target of interest.

The probe is thereby designed in a fashion that enables it to be detected both in SIMS and in fluorescence microscopy, to enable users to optimize their sample labelling using fluorescence imaging, before turning to the more laborious SIMS experiments.

After accomplishing the nanoprobe conjugation, we performed tests to optimize the labelling with IodLink-nanobody anti-mouse κlg. For this, we applied immunostainings on COS-7 cells with a mouse anti-α-tubulin as primary antibody and varying concentrations of IodLink-nanobody (ESI,† Fig. S2). We found that 20 nM IodLink-nanobody provides an adequate signal while maintaining a lower background level.

After demonstrating the nanoprobe's detectability and specificity by fluorescence microscopy, we turned to immunostaining on COS-7 cells, repeating the same approach as for α-tubulin but targeting the peroxisomal PMP70 protein, which is known to provide a very clear and easily recognized pattern in SIMS microscopy.[11] To increase the signal intensity to the maximum possible, we employed a signal enhancement procedure in which we immunostained the cells with a rabbit polyclonal antibody for PMP70, followed by a secondary goat anti-rabbit antibody, and finally a mouse anti-goat antibody, to which the IodLink-nanobody anti-mouse κlg was bound (Fig. 1C). The samples were then embedded in resin, sliced to a thickness of 200 nm and imaged in NanoSIMS. To obtain negative secondary ions, we selected $^{133}Cs^+$ as primary ion source and set several detectors to collect $^{12}C^{14}N^-$, $^{32}S^-$, and $^{127}I^-$ respectively (Fig. 2). $^{12}C^{14}N^-$ is the most common ion employed to visualize biological samples with NanoSIMS, providing an accurate image of nitrogen-rich cellular material such as proteins or nucleic acids.[17]

We also included $^{32}S^-$ to obtain additional information and facilitate the location of the cellular nuclei, due to its high abundance in structures such as the heterochromatin or nucleoli.[18,19] Finally, we collected $^{127}I^-$ ion signal to locate and visualize our proteins of interest labelled with IodLink-nanobody anti-mouse κlg (Fig. 2).

The iodine signal reproduces the typical distribution of the peroxisomes, showing a significantly higher signal in small dotted regions that are exclusively found in the cytoplasm, never penetrating the nucleus (Fig. 2). The unspecific signal obtained in negative control samples was negligible (Fig. 2 and ESI,† Fig. S3), suggesting that the IodLink-nanobody provides high specific labeling and low background signal for NanoSIMS imaging.

To further test the possibilities of this new nanoprobe, we performed an immunostaining for two proteins of interest, by

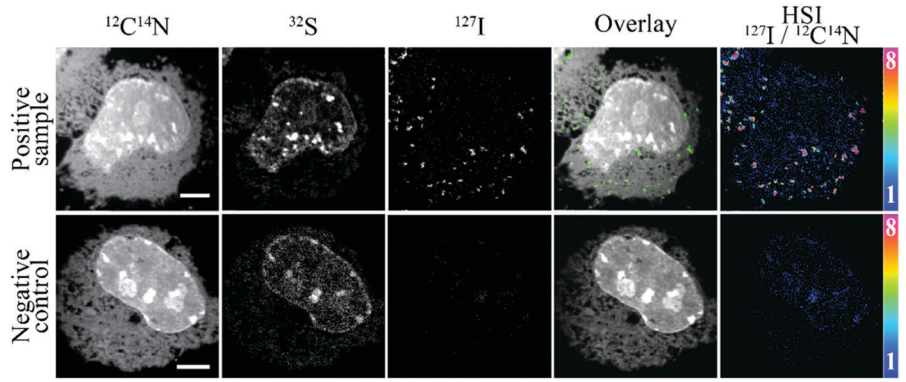

Fig. 2 NanoSIMS images of the peroxisomal PMP70 immunostained with IodLink-nanobody anti-mouse κlg. On the upper row, a cell immunostained to detect PMP70 is indicated. On the lower row, a negative control cell is shown. The negative control includes the primary antibody and IodLink-nanobody anti-mouse κlg, but skipping the incubations with the intermediate antibodies. From left to right: $^{12}C^{14}N^-$, $^{32}S^-$, $^{127}I^-$ images, overlay of $^{12}C^{14}N^-$ (grey) and $^{127}I^-$ (green), and HSI image of $^{127}I^-/^{12}C^{14}N^-$ (colour scale: magenta = maximum; blue = minimum). Scale bars: 5 μm.

combining IodLink-nanobody anti-mouse κlg with the FluorLink-nanobodies that we developed in the past.[11] The mass dispersion range offered by the NanoSIMS 50L instrument allows the simultaneous detection of $^{127}I^-$ and other mass peaks, such as $^{12}C^{14}N^-$ and $^{19}F^-$, which enabled us to analyse the mitochondrial marker (TOM70) linked to a green fluorescent protein (GFP) on COS-7 cells, using FluorLink-nanobodies anti-GFP #1 and #2, while we employed IodLink-nanobody to label the peroxisomal marker PMP70 (Fig. 3). Both probes could be introduced simultaneously through a single immunolabelling incubation step. The resulting negative ion mode NanoSIMS images showed that this procedure determines with relative ease the distribution of two proteins of interest. The regions enriched with ^{127}I and ^{19}F indicated that there were no interferences between FluorLink and IodLink probes as they showed typical patterns for mitochondrial and peroxisomal markers, respectively (Fig. 3).

The probes seem to be highly specific, but one should still take into account the fact that IodLink contains 3 fluorine atoms delivered from the fluorophore Star635. The doubling of IodLink after coupling to the nanobody's two ectopic cysteines results in 6 fluorine atoms, which in principle could interfere with our capacity to distinguish the location of two proteins of interest if combined with FluorLink-nanobodies which deliver 52xF per target. To check this, we tested the correlation level between $^{127}I^-$ and $^{19}F^-$ within the cells, using the correlation between $^{32}S^-$ and $^{12}C^{14}N^-$ as an internal reference (ESI,† Fig. S4). With this analysis, we observed the expected a strong correlation between $^{32}S^-$ and $^{12}C^{14}N^-$, and a very weak, not significant correlation between $^{127}I^-$ and $^{19}F^-$. These results demonstrate that the signal obtained from IodLink is clearly distinguishable from the FluorLink. This is in line with our previous observations, when we noticed that NanoSIMS imaging cannot solely rely on the fluorine atoms of the fluorophore Star635 to reveal the localization of proteins of interest, due to its low number of F atoms.

These experiments imply that iodine-based SIMS imaging is feasible, and can also be employed in multi-targeted proteins

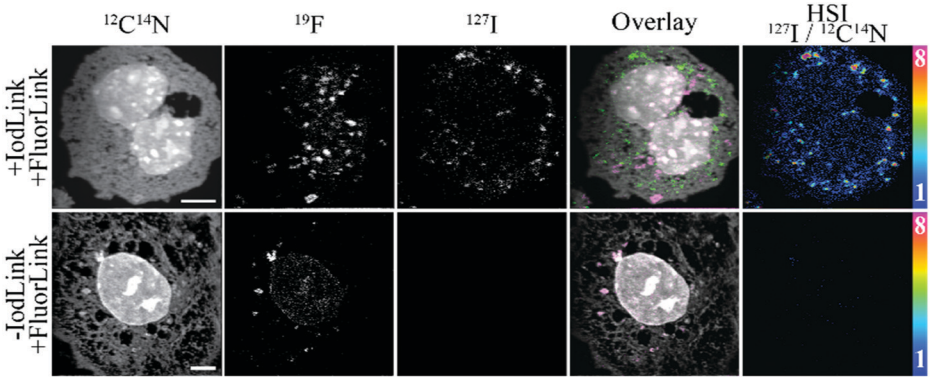

Fig. 3 NanoSIMS images of a dual-isotope immunostaining using FluorLink- and IodLink-nanobodies. TOM70-GFP transfected COS-7 cells were labelled with FluorLink-nanobodies against GFP, and the protein PMP70 was immunostained with antibodies that were detected using the IodLink-nanobody anti-mouse κlg, as above. From left to right: $^{12}C^{14}N^-$, $^{19}F^-$, $^{127}I^-$ images, overlay of $^{12}C^{14}N^-$ (grey), $^{19}F^-$ (magenta) and $^{127}I^-$ (green), and HSI image of $^{127}I^-/^{12}C^{14}N^-$ (colour scale: magenta = maximum; blue = minimum). On the upper row, representative cells stained with the entire sequence of antibodies. The lower row represents the negative control, which was labelled with the fluorine probe, as well as with the primary antibody and IodLink-nanobody anti-mouse κlg, but excludes the intermediate antibodies for the IodLink immunostaining. Scale bars: 5 μm.

imaging with NanoSIMS by combining it with other elements, detectable in negative ion mode, such as fluorine. In comparison to other elements, iodine offers a very sparse endogenous presence within biological samples. Fluorine, for example, is a prominent element in the production of detergents and plastics, including the common tubes and reagent holders used in biomedical sciences.[20] This implies that the background level for iodine tends to be much lower than for fluorine, as we can appreciate in the double staining images, in which a low fluorine signal can be observed throughout the samples.

This work demonstrates the synthesis of IodLink, a non-radioactive, stable iodine-containing probe, which can be conjugated to different surfaces or proteins bearing an accessible thiol group. To show its applicability, we successfully conjugated IodLink to an anti-mouse-nanobody, indicating the feasibility of labelling specific proteins of interest, as well as the visualization and location of such proteins by both fluorescence microscopy and SIMS.

In our work, we also demonstrated that IodLink-nanobody was effective for specific protein imaging with NanoSIMS at subcellular resolution due to its high specificity and high signal-to-noise ratio, even in dual-protein targeted imaging. Future experiments combining additional probes, also detectable on the negative secondary ion mode of SIMS, such as gold-conjugated nanobodies, could further increase the number of proteins simultaneously visualized by SIMS. In the same manner, all of these probes are compatible with the use of other isotopes such as ^{13}C, ^{15}N or ^{18}O, to study in parallel different cellular metabolic processes, such as the turnover of proteins or lipids.[21–24] Importantly, IodLink could also be detected by other SIMS instruments such as ToF-SIMS. Likewise, IodLink could be tested on other imaging techniques such as X-ray scattering, implying that this probe, while only showcased here for its application to NanoSIMS, should enable substantially more applications in the future.

S. K. G. and S. O. R. conceptualized the project. S. K. G. performed all chemistry work. S. S. I. performed the immunolabelling experiments and fluorescence imaging. F. O provided materials and supervised nanobody conjugation and their applications in IF. S. J. performed the plastic embedding. P. A. G. performed the SIMS imaging and N. T. N. P. supervised all SIMS work. P. A. G. and S. O. R. analysed the data. S. K. G., P. A. G. and S. O. R. wrote the initial draft.

We thank Prof. Dr Ulf Diederichsen (Institute of Organic and Biomolecular Chemistry, University of Göttingen, Germany) for the generous support by using his infrastructure. We also acknowledge the service department of the faculty of chemistry (University Göttingen, Germany), especially Dr. Holm Frauendorf and his team for the mass spectrometric measurements. This work was supported by grants to S. O. R. from the German Research Foundation (Deutsche Forschungsgemeinschaft, DFG SFB1286/A03, RI 1967/7-3, RI 1967/11-1) and from the Nieders. Vorab (76251-12-6/19/ZN 3458). Also supported under Germany's Excellence Strategy-EXC 2067/1-390729940. Silvio O. Rizzoli and Felipe Opazo have received compensation as consultants of NanoTag Biotechnologies GmbH and own stocks in the company.

Conflicts of interest

The other authors declare no competing interests.

Notes and references

1 M. J. Taylor, J. K. Lukowski and C. R. Anderton, *J. Am. Soc. Mass Spectrom.*, 2021, **32**, 872–894.
2 A. P. Bowman, R. M. A. Heeren and S. R. Ellis, *TrAC, Trends Anal. Chem.*, 2019, **120**, 115197.
3 P. Agüi-Gonzalez, S. Jähne and N. T. N. Phan, *J. Anal. At. Spectrom.*, 2019, **34**, 1355–1368.
4 S. G. Boxer, M. L. Kraft and P. K. Weber, *Annu. Rev. Biophys.*, 2009, **38**, 53–74.
5 J. Malherbe, F. Penen, M.-P. Isaure, J. Frank, G. Hause, D. Dobritzsch, E. Gontier, F. Horréard, F. Hillion and D. Schaumlöffel, *Anal. Chem.*, 2016, **88**, 7130–7136.
6 B. L. Gorman and M. L. Kraft, *Anal. Chem.*, 2020, **92**, 1645–1652.
7 R. L. Wilson, J. F. Frisz, W. P. Hanafin, K. J. Carpenter, I. D. Hutcheon, P. K. Weber and M. L. Kraft, *Bioconjug. Chem.*, 2012, **23**, 450–460.
8 M. Angelo, S. C. Bendall, R. Finck, M. B. Hale, C. Hitzman, A. D. Borowsky, R. M. Levenson, J. B. Lowe, S. D. Liu, S. Zhao, Y. Natkunam and G. P. Nolan, *Nat. Med.*, 2014, **20**, 436–442.
9 I. C. Vreja, S. Kabatas, S. K. Saka, K. Kröhnert, C. Höschen, F. Opazo, U. Diederichsen and S. O. Rizzoli, *Angew. Chem., Int. Ed.*, 2015, **54**, 5784–5788.
10 S. Kabatas, I. C. Vreja, S. K. Saka, C. Höschen, K. Kröhnert, F. Opazo, S. O. Rizzoli and U. Diederichsen, *Chem. Commun.*, 2015, **51**, 13221–13224.
11 S. Kabatas, P. Agüi-Gonzalez, R. Hinrichs, S. Jähne, F. Opazo, U. Diederichsen, S. O. Rizzoli and N. T. N. Phan, *J. Anal. At. Spectrom.*, 2019, **34**, 1083–1087.
12 P. Agüi-Gonzalez, T. M. Dankovich, S. O. Rizzoli and N. T. N. Phan, *Nanomaterials*, 2021, **11**, 1797.
13 S. Kabatas, P. Agüi-Gonzalez, K. Saal, S. Jähne, F. Opazo, S. O. Rizzoli and N. T. N. Phan, *Angew. Chem., Int. Ed.*, 2019, **58**, 3438–3443.
14 P. F. Lang and B. C. Smith, *J. Chem. Educ.*, 2010, **87**, 875–881.
15 T. Andersen, H. K. Haugen and H. Hotop, *J. Phys. Chem. Ref. Data*, 1999, **28**, 1511–1533.
16 C. E. Citterio, H. M. Targovnik and P. Arvan, *Nat. Rev. Endocrinol.*, 2019, **15**, 323–338.
17 M. L. Steinhauser and C. P. Lechene, *Semin. Cell Dev. Biol.*, 2013, **24**, 661–667.
18 A. A. Legin, A. Schintlmeister, M. A. Jakupec, M. Galanski, I. Lichtscheidl, M. Wagner and B. K. Keppler, *Chem. Sci.*, 2014, **5**, 3135–3143.
19 F. Lange, P. Agüi-Gonzalez, D. Riedel, N. T. N. Phan, S. Jakobs and S. O. Rizzoli, *PLoS One*, 2021, **16**, e0240768.
20 S. Banerjee, *Handbook of Specialty Fluorinated Polymers*, Elsevier, 2015.
21 S. K. Saka, A. Vogts, K. Kröhnert, F. Hillion, S. O. Rizzoli and J. T. Wessels, *Nat. Commun.*, 2014, **5**, 3664.
22 S. Jähne, F. Mikulasch, H. G. H. Heuer, S. Truckenbrodt, P. Agüi-Gonzalez, K. Grewe, A. Vogts, S. O. Rizzoli and V. Priesemann, *Cell Rep.*, 2021, **34**, 108841.
23 M. L. Kraft and H. A. Klitzing, *Biochim. Biophys. Acta*, 2014, **1841**, 1108–1119.
24 C. He, X. Hu, R. S. Jung, T. A. Weston, N. P. Sandoval, P. Tontonoz, M. R. Kilburn, L. G. Fong, S. G. Young and H. Jiang, *Proc. Natl. Acad. Sci. U. S. A.*, 2017, **114**, 2000–2005.